Hindawi Publishing Corporation
Journal of Nanomaterials
Volume 2013, Article ID 135147, 7 pages
http://dx.doi.org/10.1155/2013/135147

Research Article

Application of Flower-Like ZnO Nanorods Gas Sensor Detecting SF_6 Decomposition Products

Shudi Peng, Gaolin Wu, Wei Song, and Qian Wang

Chongqing Electric Power Research Institute, Chongqing 401123, China

Correspondence should be addressed to Shudi Peng; psdzq@yahoo.cn

Received 21 November 2012; Accepted 3 January 2013

Academic Editor: Wen Zeng

Gas insulated switchgear (GIS) is an important electric power equipment in a substation, and its running state has a significant relationship with stability, security, and reliability of the whole electric power system. Detecting and analyzing the decomposition byproducts of sulfur hexafluoride gas (SF_6) is an effective method for GIS state assessment and fault diagnosis. This paper proposes a novel gas sensor based on flower-like ZnO nanorods to detect typical SF_6 decompositions. Flower-like ZnO nanoparticles were synthesized via a simple hydrothermal method and characterized by X-ray powder diffraction and field-emission scanning electron microscopy, respectively. The gas sensor was fabricated with a planar-type structure and applied to detect SF_6 decomposition products. It shows excellent sensing properties to SO_2, SOF_2, and SO_2F_2 with rapid response and recovery time and long-term stability and repeatability. Moreover, the sensor shows a remarkable discrimination among SO_2, SOF_2, and SO_2F_2 with high linearity, which makes the prepared sensor a good candidate and a wide application prospect detecting SF_6 decomposition products in the future.

1. Introduction

Gas insulated switchgear (GIS) filled with pressurized sulfur hexafluoride gas (SF_6) is widely used in electric power system in recent decades with the advantages of small floor space, high stability and reliability, high-strength insulation, none smeary oil, lower maintenance cost, and so on [1–6]. Sulfur hexafluoride gas has excellent insulating performance and arc extinction function, and it can dramatically improve the insulation intensity when used as an insulating medium. So it is widely applied to GIS and other gas insulation equipments [1, 3]. However, there exist some unavoidable insulating defects in the process of GIS design, manufacture, installation, and operation [4].

As an inert gas, pure SF_6 is colorless, tasteless, nontoxic, and noninflammable, and its decomposition temperature is as high as 500°C [7]. Although SF_6 is of great chemical inertness and the reliability of GIS is very high, inevitable insulating faults based on arc discharge, spark discharge, or partial discharge may occur due to the internal insulating defects. Researches both at home and aboard demonstrate that such internal insulation faults would cause SF_6 gas to decompose, and generate several kinds of low-fluorine sulfides, such as SF_4, SF_3, and SF_2 [2, 4, 5, 8, 9]. If the SF_6 in GIS is pure, the decomposed low-fluorine sulfides will reduce to SF_6 fast with the decrease of operating temperature. Actually, it always contains a certain amount of impurities, such as air and water. Some low-fluorine sulfides are very active to react with trace moisture and oxygen and generate the compounds of SOF_4, SOF_2, SO_2F_2, SO_2, HF, and so on. As the GIS insulating defects vary, the decomposed gas mixtures will be different. And the composition contents and decomposition rates are also various. Therefore, detecting and analyzing the decomposed chemical byproducts accurately can efficiently identity and diagnose fault type occurred in GIS.

At present, many methods [10–13] are used to detect the SF_6 decomposition components in GIS, for instance, gas chromatography, gas detection tube, infrared absorption spectrometry, and semiconductor gas sensor. Gas chromatography [10] is mainly used for offline testing and it takes a quite long time. Gas detection tube [11] has no response to some decomposition components and its stability depends on environment condition. Infrared absorption spectrometry [12, 13] has cross-response on SF_6 and cannot quantitatively

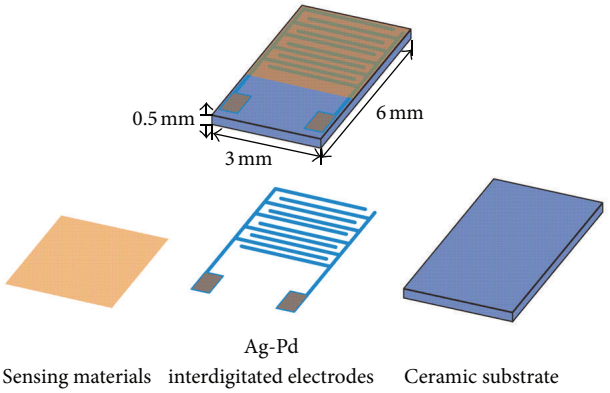

Figure 1: Schematic representation of planar ZnO gas sensor structure.

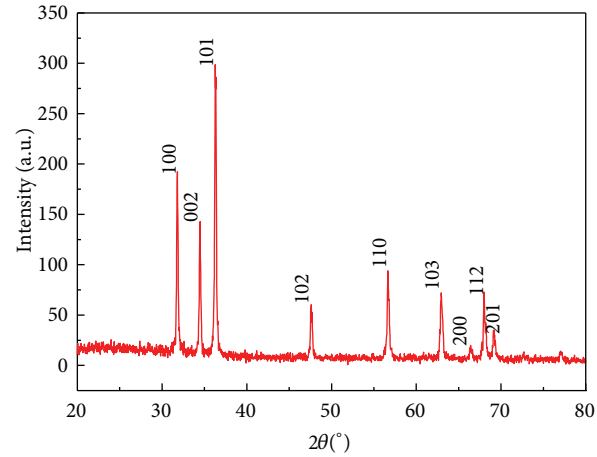

Figure 2: XRD patterns of the ZnO nanorods.

detect the decomposition components. In recent years, metal oxide semiconductor gas sensor based on ZnO [14], SnO_2 [15], TiO_2 [16], Fe_2O_3 [17], WO_3 [18], or In_2O_3 [19] has been widely used for detecting and online monitoring target gas, owing to advantages of simple fabrication process, rapid response and recovery time, low maintenance cost, long service life, long-term stability and repeatability, and so on. With the development of nanotechnology, various gas sensors have been fabricated with small particle size and high surface-to-volume ratio [20]. However, most of these gas sensors mainly focus on toxic gas [21, 22], organic gas [23, 24], carbon dioxide [25], hydrogen [26], and rare studies concerning the SF_6 decompositions. Meanwhile, the cross-sensitivity among the decomposition components is tough, so investigating sensing properties especially selectivity is the most crucial issue for online monitoring SF_6 decompositions.

In this work, we proposed a simple and effective hydrothermal synthesis route to prepare flower-like ZnO nanorods. X-ray powder diffraction (XRD) and field-emission scanning electron microscopy (FESEM) were used to characterize the microstructures and morphologies of the prepared samples. Then a gas sensor based on the flower-like ZnO nanorods was fabricated, and its gas sensing properties against SF_6 decompositions were investigated. Particularly, the study mainly focused on the sensing behaviors of the prepared sensor against SOF_2, SO_2F_2, and SO_2, and its cross-sensitivity was also demonstrated. The prepared sensor exhibited excellent gas response to different SF_6 decompositions at different working temperature with high linearity, rapid response-recovery, and long-time stability and repeatability.

2. Experimental

2.1. Preparation and Characterization of ZnO Nanorods. Flower-like zinc oxide nanorods samples were successfully synthesized through a hydrothermal method using ammonium hydroxide (NH_4OH, 28 wt% NH_3 in H_2O) as the base source and zinc nitrate hexahydrate ($Zn(NO_3)_2{\cdot}6H_2O$) as the source of Zn^{2+} ions. All chemicals were of analytical reagent grade and purchased from Beijing Chemicals Co., Ltd. In a typical synthesis process, an adequate amount of $Zn(NO_3)_2{\cdot}6H_2O$ was dissolved in deionized water (DI water) with a large beaker, and NH_4OH was added slowly to the solution under intense magnetic stirring. The mixed solution was stirred for 30 min and then transferred into a sealed Teflon autoclave with 100 mL of inner volume and 80% of fill ratio. After 24 h reaction at 180°C, the reactor was cooled to room temperature naturally. Subsequently, the prepared white products were centrifuged, washed two or three times with DI water and ethanol alternately, and dried at 80°C in air for further use.

XRD analysis was conducted on a Rigaku D/max-2500 X-ray diffractometer with the 2θ range of 20–80°C at room temperature, and Cu $K_{\alpha 1}$ as the source of X-ray at 40 kV, 40 mA, and λ = 1.5418 Å. FESEM images were performed on a JEOL JEM-6700F microscope operating at 3 and 5 kV, respectively.

2.2. Fabrication and Measurement of ZnO Sensor. ZnO nanorods gas sensor was fabricated based on a planar construction with a simple and convenient fabrication procedure. The scheme of the planar ZnO gas sensor structure was shown in Figure 1, where prepared planar ZnO nanorods gas sensor is constituted of planar ceramic substrate, Ag-Pd interdigitated electrodes, and sensing material. The length, width, and height of the planar ceramic substrate are suggested to be about 6, 3, and 0.5 mm, respectively. There are five pairs of Ag-Pd interdigitated electrodes on planar ceramic substrate with both width and distance about 0.15 mm. As-prepared samples were further ground into fine powder and mixed with diethanolamine and ethanol to form a paste with a weight ratio of 100 : 10 : 10. It was subsequently screen printed onto the planar ceramic substrate to form a sensing film and the thickness was about 10 um and then dried in air at 60°C for 5 h. Finally, the sensor was further aged at an aging test chamber for 240 h.

Gas sensing properties of the prepared planar ZnO gas sensor to SF_6 decomposition byproducts were investigated using an intelligent gas detecting system. Targeted gases were

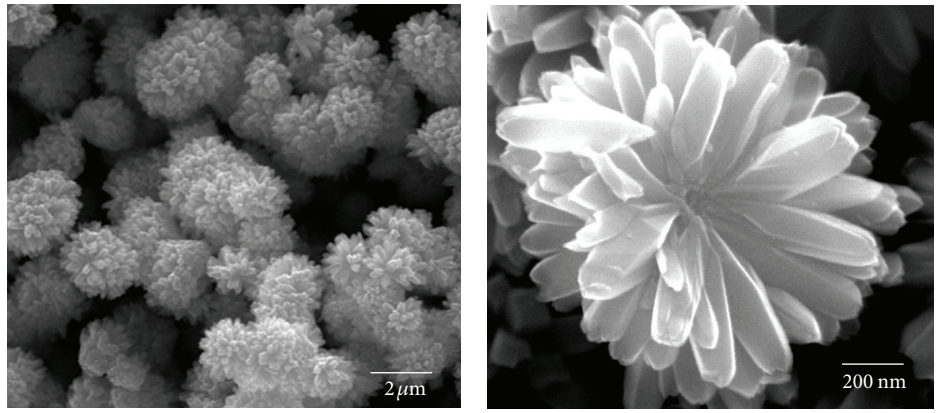

FIGURE 3: (a) Low-resolution FESEM image and (b) high-resolution FESEM image of the ZnO nanorods.

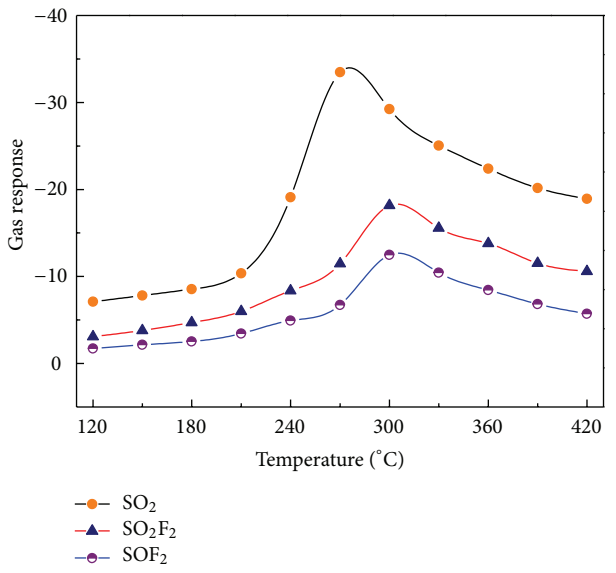

FIGURE 4: Gas response versus temperature curves to 50 μL/L of SO_2, SOF_2, and SO_2F_2.

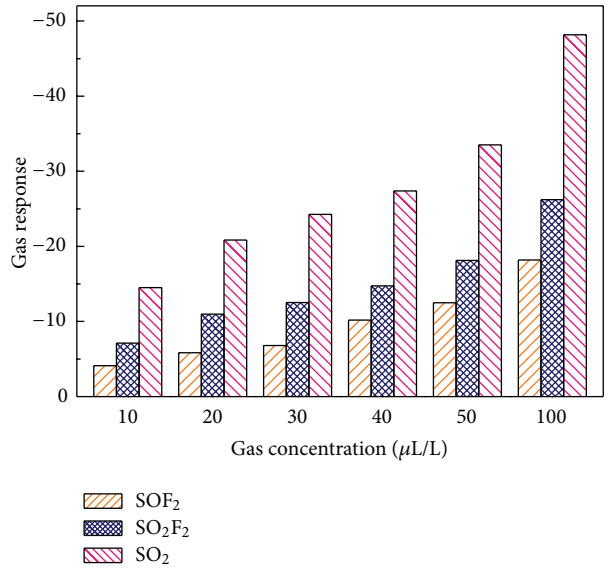

FIGURE 5: Gas response versus concentrations curves to SO_2, SOF_2, and SO_2F_2.

mixed with N_2 by a dynamic gas distributing system which worked with high accuracy mass flow controllers and then injected into the gas sensing chamber. The concentration of detecting gas was controlled and detected by gas mass flow meter. The operating temperature of the gas sensor was controlled by varying current flow of the heater. And the surface temperature of the planar sensor was measured by a thermocouple in real time. When the testing sensor was preheated at 300°C for some time in air and the baseline of resistance was smooth and stable, we could start our gas sensing properties test.

Gas response was defined as the relative variation of the electrical resistance of the gas sensor: $S\% = (R - R_0)/R_0 \times 100\%$. R is the resistance of flower-like ZnO nanorods gas sensor in target gas environment and R_0 being in pure air. The response time was defined as the time taken by the sensor to achieve 90% of the total resistance change in the case of gas in or the recovery time in the case of gas out. All experiments were repeated several times to ensure the reproducibility and stability of the sensor.

3. Results and Discussion

3.1. Structure and Morphology. Figure 2 shows the XRD patterns of the as-prepared ZnO nanorods. All the diffraction peaks are consistent with the values in the standard card (JCPDS 36-1451) and can be indexed as typical wurtzite hexagonal ZnO crystal structure with lattice constants $a = 3.249$ Å and $c = 5.206$ Å. No other diffraction peaks from any impurities are detected.

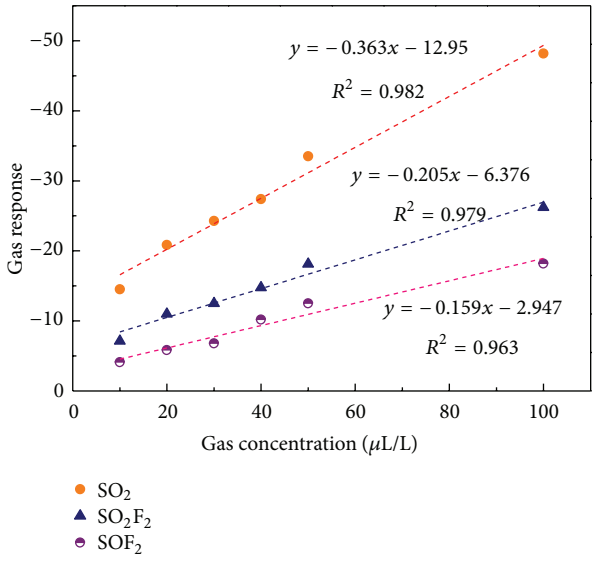

FIGURE 6: The linear calibration curves of SO_2, SOF_2, and SO_2F_2.

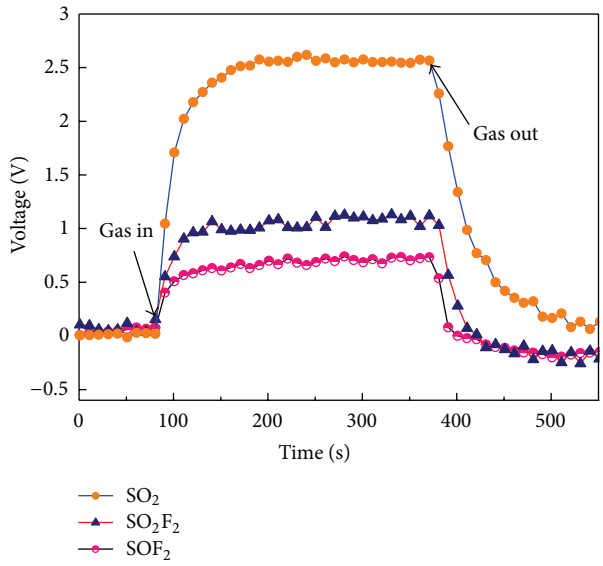

FIGURE 7: The response and recovery behaviors of the sensor to 10 μL/L of SO_2, SOF_2, and SO_2F_2.

Figures 3(a) and 3(b) are typical low-resolution and high-resolution FESEM images of the prepared flower-like ZnO nanorods samples synthesized with the hydrothermal method. The nanoparticles have a high uniform flower-like bundle structure and self-assemble into flowers. The average length of ZnO nanorods is about 400 nm with an aspect ratio of 4 : 1.

3.2. Gas Sensing Properties and Sensing Mechanism. The gas sensing performances of metal oxide semiconductor gas sensor are dominantly influenced by working condition. Gas sensing experiments are performed with an intelligent gas detecting system at different operating temperatures to find out the optimum working temperature. Figure 4 shows the gas responses of the prepared flower-like ZnO nanorods gas sensor against 50 μL/L of SF_6 compositions as a function of operating temperature, which ranges from 120°C to 420°C. As seen in Figure 4, the measured gas response curves have a common change trend, in which gas response increases firstly with rising operating temperature and reaches the maximum, and then decreases with an continuous increase of the operating temperature.

This behavior can be understood by a dynamic equilibrium mechanism between gas adsorption and desorption process of gas molecule on the surface of ZnO or other similar semiconducting metal oxides. In the beginning, the rate of gas adsorption is much higher than that of desorption, and the amount of net adsorbed gas increases as the operating temperature rises. It would reach a saturated adsorption state and maintain a dynamic balance at the constant operating temperature. With a sequential increase of the operating temperature, the balance will be broken and it changes to a net desorption process, which ultimately results in a decreasing gas response. As shown in Figure 4, the optimal operating temperatures of the sensor to 50 μL/L of SO_2, SOF_2, and SO_2F_2 are 250, 300, and 300°C with gas response of −33.44, −12.47, and −18.06, respectively, which are applied in all the following investigations in this paper.

At their optimal operating temperatures, we performed the gas responses of the prepared plane flower-like ZnO gas sensor against different concentrations of SO_2, SOF_2, and SO_2F_2. Figure 5 shows the relationship between gas responses and 10, 20, 30, 40, 50, and 100 μL/L of SO_2, SOF_2, and SO_2F_2, respectively. The gas response measured is manifested to persistently increase with a rising gas concentration. At the same level of gas concentration, the gas response values of the sensor to the three targeted gases decrease in the order of SO_2, SO_2F_2, and SOF_2.

If the gas response curve is linear or quasilinear, the sensor can be applied to engineering application in practice. Therefore, based on the linear fitting tool in Origin software, linear characteristics of the prepared sensor to SO_2, SO_2F_2, and SOF_2 were discussed. Figure 6 shows the linear calibration curves of the sensor to SO_2, SO_2F_2, and SOF_2 with gas concentrations in the range of 10–100 μL/L. As seen in Figure 6, all the three gas response curves meet highly linear with gas concentration, and the linear correlation coefficient R^2 for SO_2, SO_2F_2, and SOF_2 is suggested to be about 0.982, 0.979, and 0.963, respectively. Such a higher linear dependence indicates that our prepared flower-like ZnO gas sensor can be used as promising materials for detecting SF_6 decompositions such as SO_2, SO_2F_2, and SOF_2.

Response time and recovery time are other two key indicators to evaluate gas sensor performances. Figure 7 shows the response and recovery characteristic of the prepared sensor to 10 μL/L of SO_2, SO_2F_2, and SOF_2 with the sensor working at its optimum operating temperature. As shown in Figure 7, the response times for 10 μL/L of SO_2, SO_2F_2, and SOF_2 are about 21, 13, and 10 s, and correspondingly the recovery times are about 45, 32, and 17 s, respectively.

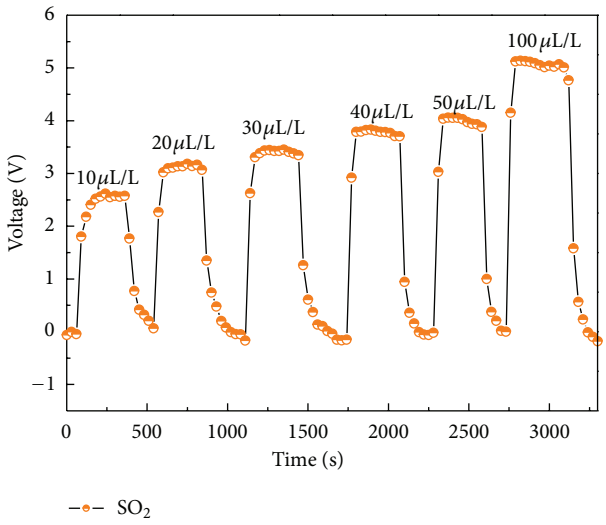

FIGURE 8: The response and recovery behaviors of the sensor to SO_2.

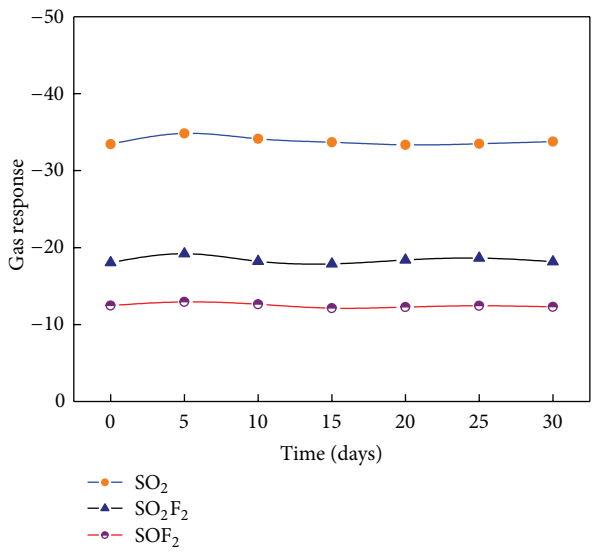

FIGURE 9: The stability and repeatability of the sensor against 50 μL/L of SO_2, SO_2F_2, and SOF_2.

Such rapid response and recovery characteristic could be ascribed to the structure of the prepared flower-like sensor, which has a much bigger specific surface area than other conventional sensing structures, provides a larger adsorption area, and increases the amount of gas molecules adsorbed on the surface. Those advantages increase the rate of charge carriers and facilitate the movement of carriers through the barriers, consequently fast response and response property are observed.

The response and recovery behaviors versus SO_2 with concentration at 10, 20, 30, 40, 50, and 100 μL/L are shown in Figure 8. With the concentration of detected gas increasing, the gas response amplitude increases apparently, nevertheless the response and recovery property changes slightly which indicates a very good and satisfying reproducibility of prepared sensor against the decompositions. Figure 9 shows the long-term stability and repeatability of the sensor against 50 μL/L of SO_2, SO_2F_2, and SOF_2. One can clearly see in Figure 9 that the gas response changes slightly and keeps at a nearly constant value during the long experimental cycles, which confirms the excellent longtime stability and repeatability of the prepared flower-like ZnO nanorods gas sensor for detecting SO_2, SO_2F_2, and SOF_2.

For most metal oxide semiconductor gas sensors such as zinc oxide, tin oxide, titanium oxide, ferric oxide, and indium oxide, the sensing properties are dominantly controlled by the change of electrical resistance [27], which is fundamentally attributed to the chemical adsorption and desorption process of gas molecules on sensing surface of the sensor.

It is well known to all that zinc oxide is a typical n-type semiconducting material and there exist many oxygen vacancies in the crystal lattices [28–30], where various kinds of oxygen could be adsorbed. The species of adsorbed oxygen are closely related to the ambient temperature [31]. At room temperature, oxygen is likely to be adsorbed on ZnO surface or grain boundaries with a typical physical adsorption mode. And it would turn into chemical adsorption by thermal excitation or electric excitation with certain energy.

As shown in Figure 10(a), oxygen would capture electrons and form a depletion region on the surface area, which results in a decrease in the concentration of charge carrier and electron mobility, thus gas sensor shows a higher electrical resistance. Figure 10(b) illustrates the gas sensing process of SO_2 as an example exploring the gas sensing mechanism of the prepared sensor detecting SF_6 decompositions. When flower-like ZnO nanorods are reducing gas ambient at moderate temperature (such as in certain concentration of SO_2, SO_2F_2, and SOF_2), the reducing gas reacts with chemical adsorbed oxygen, and then trapped electrons would be released back into ZnO surface. Electrons released from chemical adsorbed oxygen would reduce the height of barriers in the depletion region and increase the number of charge carriers [32, 33], which promotes the movements of charge carriers between conduction band and valence band and eventually increases the electrical conductivity of the sensor [34, 35].

With temperature rising, chemical adsorbed oxygen exists in various forms, namely, O_{2ads}^-, O_{ads}^-, and O_{ads}^{2-}, as shown in the following reaction equations:

$$\begin{aligned} &O_{2gas} \longrightarrow O_{2ads} \qquad O_{2ads} + e^- \longrightarrow O_{2ads}^- \\ &O_{2ads}^- + e^- \longrightarrow 2O_{ads}^- \qquad O_{ads}^- + e^- \longrightarrow O_{ads}^{2-} \end{aligned} \tag{1}$$

As mentioned above the state of adsorbed oxygen is mainly determined by the ambient temperature. At lower experimental temperatures, oxygen dominantly exists in the form of a "molecular ion" O_{2ads}^- and transfers into "atomic ion" O_{ads}^- and O_{ads}^{2-} with a further rising operating temperature. Experimental results indicate that the transition temperature for oxygen from "molecular ion" to "atomic ion" is about 450~500 K. As performed in Figure 4, the optimum

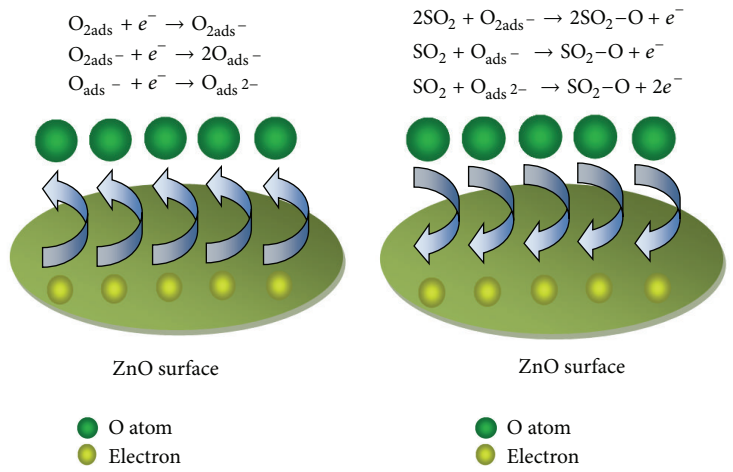

(a) Oxygen adsorbed on ZnO surface. (b) SO_2 gas sensing on ZnO surface ZnO

FIGURE 10: Schematic plot illustrating the sensing mechanism of prepared sensor to SO_2.

working temperatures for SO_2, SO_2F_2, and SOF_2 are about 250, 300, and 300°C, respectively. Thus, we draw a conclusion that the sensing behavior of the prepared sensor to SO_2 gas may belong to the "molecular ion" reaction pattern, while it is an "atomic ion" gas response mode for SO_2F_2 and SOF_2.

4. Conclusions

In summary, Flower-like ZnO nanorods have been successfully synthesized and characterized by XRD and FESEM. The optimum operating temperatures of the prepared sensor to SO_2, SO_2F_2, and SOF_2 are about 250, 300, and 300°C. The response (recovery) time of the sensor to 10 μL/L of SO_2, SO_2F_2, and SOF_2 is 21 (45), 13 (32), and 10 (17) s, respectively. Especially, the flower-like ZnO nanorods gas sensor shows high linearity to SO_2, SO_2F_2, and SOF_2 at the range of 10–100 μL/L with excellent linear correlation coefficient R^2 at 0.982, 0.979, and 0.963, separately. These findings demonstrate that our prepared flower-like ZnO nanorods have some excellent potential advantages for using as gas sensors to detect and online monitor the SF_6 decompositions such as SO_2, SOF_2, and SO_2F_2 in practice, although further studies are still needed.

References

[1] J. Tang, F. Liu, X. X. Zhang, Q. H. Meng, and J. B. Zhou, "Partial discharge recognition through an analysis of SF_6 decomposition products Part 1: decomposition characteristics of SF_6 under four different partial discharges," *IEEE Transactions on Dielectrics and Electrical Insulation*, vol. 19, no. 1, pp. 29–36, 2012.

[2] M. Shih, W. J. Lee, and C. Y. Chen, "Decomposition of SF_6 and H_2S mixture in radio frequency plasma environment," *Industrial and Engineering Chemistry Research*, vol. 42, no. 13, pp. 2906–2912, 2003.

[3] J. Tang, F. Liu, X. X. Zhang, Q. H. Meng, and J. G. Tao, "Partial discharge recognition through an analysis of SF_6 decomposition products part 2: feature extraction and decision tree-based pattern recognition," *IEEE Transactions on Dielectrics and Electrical Insulation*, vol. 19, no. 1, pp. 37–44, 2012.

[4] R. J. Van Brunt and J. T. Herron, "Fundamental processes of SF_6 decomposition and oxidation in glow and corona discharges," *IEEE Transactions on Electrical Insulation*, vol. 25, no. 1, pp. 75–94, 1990.

[5] M. Shih, W. J. Lee, C. H. Tsai, P. J. Tsai, and C. Y. Chen, "Decomposition of SF_6 in an RF plasma environment," *Journal of the Air and Waste Management Association*, vol. 52, no. 11, pp. 1274–1280, 2002.

[6] I. Sauers, H. W. Ellis, and L. G. Christophorou, "Neutral decomposition products in spark breakdown of SF_6," *IEEE Transactions on Electrical Insulation*, vol. EI-21, no. 2, pp. 111–120, 1986.

[7] W. T. Tsai, "The decomposition products of sulfur hexafluoride (SF_6): reviews of environmental and health risk analysis," *Journal of Fluorine Chemistry*, vol. 128, no. 11, pp. 1345–1352, 2007.

[8] L. Vial, A. M. Casanovas, I. Coll, and J. Casanovas, "Decomposition products from negative and 50 Hz ac corona discharges in compressed SF_6 and SF_6/N_2 (10 : 90) mixtures. Effect of water vapour added to the gas," *Journal of Physics D*, vol. 32, no. 14, pp. 1681–1692, 1999.

[9] C. T. Dervos and P. Vassiliou, "Sulfur hexafluoride (SF_6): Global environmental effects and toxic byproduct formation," *Journal of the Air and Waste Management Association*, vol. 50, no. 1, pp. 137–141, 2000.

[10] E. Duffour, "Molecular dynamic simulations of the collision between copper ions, SF_6 molecules and a polyethylene surface: a study of decomposition products and an evaluation of the self-diffusion coefficients," *Macromolecular Theory and Simulations*, vol. 19, no. 2-3, pp. 88–99, 2010.

[11] J. I. Baumbach, P. Pilzecker, and E. Trindade, "Monitoring of circuit breakers using ion mobility spectrometry to detect SF_6-decomposition," *International Journal for Ion Mobility Spectrometry*, vol. 2, no. 1, pp. 35–39, 1999.

[12] R. Kurte, C. Beyer, H. M. Heise, and D. Klockow, "Application of infrared spectroscopy to monitoring gas insulated high-voltage equipment: electrode material-dependent SF_6 decomposition,"

Analytical and Bioanalytical Chemistry, vol. 373, no. 7, pp. 639–646, 2002.

[13] W. Ding, R. Hayashi, K. Ochi et al., "Analysis of PD-generated SF_6 decomposition gases adsorbed on carbon nanotubes," *IEEE Transactions on Dielectrics and Electrical Insulation*, vol. 13, no. 6, pp. 1200–1207, 2006.

[14] J. Singh, A. Mukherjee, S. K. Sengupta, J. Im, G. W. Peterson, and J. E. Whitten, "Sulfur dioxide and nitrogen dioxide adsorption on zinc oxide and zirconium hydroxide nanoparticles and the effect on photoluminescence," *Applied Surface Science*, vol. 258, no. 15, pp. 5778–5785, 2012.

[15] B. Wang, L. F. Zhu, Y. H. Yang, N. S. Xu, and G. W. Yang, "Fabrication of a SnO_2 nanowire gas sensor and sensor performance for hydrogen," *Journal of Physical Chemistry C*, vol. 112, no. 17, pp. 6643–6647, 2008.

[16] J. Gong, Y. Li, Z. Hu, Z. Zhou, and Y. Deng, "Ultrasensitive NH_3 gas sensor from polyaniline nanograin enchased TiO_2 fibers," *Journal of Physical Chemistry C*, vol. 114, no. 21, pp. 9970–9974, 2010.

[17] X. Liu, J. Zhang, X. Guo, S. Wu, and S. Wang, "Porous α-Fe_2O_3 decorated by Au nanoparticles and their enhanced sensor performance," *Nanotechnology*, vol. 21, no. 9, Article ID 095501, 2010.

[18] B. Cao, J. Chen, X. Tang, and W. Zhou, "Growth of monoclinic WO_3 nanowire array for highly sensitive NO_2 detection," *Journal of Materials Chemistry*, vol. 19, no. 16, pp. 2323–2327, 2009.

[19] S. E. Moon, H. Y. Lee, J. Park et al., "Low power consumption and high sensitivity carbon monoxide gas sensor using indium oxide nanowire," *Journal of Nanoscience and Nanotechnology*, vol. 10, no. 5, pp. 3189–3192, 2010.

[20] W. Zeng, T. Liu, Z. Wang, S. Tsukimoto, M. Saito, and Y. Ikuhara, "Selective detection of formaldehyde gas using a Cd-Doped TiO_2-SnO_2 sensor," *Sensors*, vol. 9, no. 11, pp. 9029–9038, 2009.

[21] M. Chen, Z. Wang, D. Han, F. Gu, and G. Guo, "Porous ZnO polygonal nanoflakes: synthesis, use in high-sensitivity NO_2 gas sensor, and proposed mechanism of gas sensing," *Journal of Physical Chemistry C*, vol. 115, no. 26, pp. 12763–12773, 2011.

[22] E. Oh, H. Y. Choi, S. H. Jung et al., "High-performance NO_2 gas sensor based on ZnO nanorod grown by ultrasonic irradiation," *Sensors and Actuators B*, vol. 141, no. 1, pp. 239–243, 2009.

[23] K. Zheng, L. Gu, D. Sun, X. Mo, and G. Chen, "The properties of ethanol gas sensor based on Ti doped ZnO nanotetrapods," *Materials Science and Engineering B*, vol. 166, no. 1, pp. 104–107, 2010.

[24] A. Wei, L.-H. Pan, X.-C. Dong, and W. Huang, "Room-temperature NH_3 gas sensor based on hydrothermally grown ZnO nanorods," *Chinese Physics Letters*, vol. 28, no. 8, pp. 702–706, 2011.

[25] C. Wen, Y. Ju, W. Li et al., "Carbon dioxide gas sensor using SAW device based on ZnO film," *Applied Mechanics and Materials*, vol. 135-136, pp. 347–352, 2012.

[26] O. Lupan, G. Chai, and L. Chow, "Novel hydrogen gas sensor based on single ZnO nanorod," *Microelectronic Engineering*, vol. 85, no. 11, pp. 2220–2225, 2008.

[27] W. Zeng, T. Liu, and Z. Wang, "Enhanced gas sensing properties by SnO_2 nanosphere functionalized TiO_2 nanobelts," *Journal of Materials Chemistry*, vol. 22, no. 8, pp. 3544–3548, 2012.

[28] J. Kim and K. Yong, "Mechanism study of ZnO nanorod-bundle sensors for H_2S gas sensing," *Journal of Physical Chemistry C*, vol. 115, no. 15, pp. 7218–7224, 2011.

[29] D. Velasco-Arias, D. Díaz, P. Santiago-Jacinto, G. Rodríguez-Gattorno, A. Vázquez-Olmos, and S. E. Castillo-Blum, "Direct interaction of colloidal nanostructured ZnO and SnO_2 with NO and SO_2," *Journal of Nanoscience and Nanotechnology*, vol. 8, no. 12, pp. 6389–6397, 2008.

[30] Q. Qi, T. Zhang, Q. Yu et al., "Properties of humidity sensing ZnO nanorods-base sensor fabricated by screen-printing," *Sensors and Actuators B*, vol. 133, no. 2, pp. 638–643, 2008.

[31] M.-W. Ahn, K.-S. Park, J.-H. Heo et al., "Gas sensing properties of defect-controlled ZnO-nanowire gas sensor," *Applied Physics Letters*, vol. 93, no. 26, Article ID 263103, 2008.

[32] M. W. Ahn, K. S. Park, J. H. Heo, D. W. Kim, K. J. Choi, and J. G. Park, "On-chip fabrication of ZnO-nanowire gas sensor with high gas sensitivity," *Sensors and Actuators B*, vol. 138, no. 1, pp. 168–173, 2009.

[33] J. Zhang, S. Wang, M. Xu et al., "Hierarchically porous ZnO architectures for gas sensor application," *Crystal Growth and Design*, vol. 9, no. 8, pp. 3532–3537, 2009.

[34] Z. Yuan, X. Jiaqiang, X. Qun, L. Hui, P. Qingyi, and X. Pengcheng, "Brush-like hierarchical zno nanostructures: synthesis, photoluminescence and gas sensor properties," *Journal of Physical Chemistry C*, vol. 113, no. 9, pp. 3430–3435, 2009.

[35] J. Zhang, X. Liu, S. Wu, B. Cao, and S. Zheng, "One-pot synthesis of Au-supported ZnO nanoplates with enhanced gas sensor performance," *Sensors and Actuators B*, vol. 169, pp. 61–66, 2012.